Continuous Fatty Acid Decarboxylation using an Immobilized Photodecarboxylase in a Membrane Reactor

Zhou, Jianle; Hollmann, Frank; He, Qi; Chen, Wen; Ma, Yunjian; Wang, Yonghua

Important note
To cite this publication, please use the final published version (if applicable).
Please check the document version above.

Continuous Fatty Acid Decarboxylation using an Immobilized Photodecarboxylase in a Membrane Reactor

Jianle Zhou,[a] Frank Hollmann,[b] Qi He,[a] Wen Chen,[a] Yunjian Ma,*[a] and Yonghua Wang*[a, c]

The realm of photobiocatalytic alkane biofuel synthesis has burgeoned recently; however, the current dearth of well-established and scalable production methodologies in this domain remains conspicuous. In this investigation, we engineered a modified form of membrane-associated fatty acid photodecarboxylase sourced from *Microactinium conductrix* (*Mc*FAP). This endeavour resulted in creating an innovative assembled photoenzyme-membrane (protein load 5 mg cm^{-2}), subsequently integrated into an illuminated flow apparatus to achieve uninterrupted generation of alkane biofuels. Through batch experiments, the photoenzyme-membrane exhibited its prowess in converting fatty acids spanning varying chain lengths (C6–C18). Following this, the membrane-flow mesoscale reactor attained a maximum space-time yield of 1.2 mmol L^{-1} h^{-1} (C8) and demonstrated commendable catalytic proficiency across eight consecutive cycles, culminating in a cumulative runtime of eight hours. These findings collectively underscored the photoenzyme-membrane's capability to facilitate the biotransformation of diverse fatty acids, furnishing valuable benchmarks for the conversion of biomass via photobiocatalysis.

Introduction

Biofuels are seen as a viable alternative to fossil fuels and have great potential to contribute to the advancement of a sustainable economy.[1,2] Nevertheless, the molecular structure disparities between traditional biofuels (such as bioethanol and fatty acid methyl esters) and fossil fuels (i.e. alkanes) hinder their compatibility with commonly utilized engines.[3] In recent years, enzymatic generation of alkane biofuel from renewable fatty acids (for example, from microorganisms and non-edible oils) has emerged in the field of bioenergy.[4–6] Fatty acid photodecarboxylase (FAP), membrane-associated proteins isolated from algal chloroplasts that can convert fatty acids into C1-shortened alkane biofuels when stimulated by blue light, have emerged as a participant in the development of a new generation of biofuel.[7,8]

The light-dependency of FAP,[9] however, also brings about some practical limitations. On the one hand, the light-intensity decreases dramatically with distance from the light source (in optically transparent media the light intensity is inversely proportional to the square of the distance). This issue becomes even more pressing in turbid media where light penetration depths can be as low as a few millimetres.[10] Hence, maximizing the ration of surface area to reaction volume is desirable. Furthermore, immobilization of FAP to most commercial carriers is not straight forward as they are typically optically intransparent.[11] Finally, substrate diffusion limitations to FAP may turn out detrimental as illumination of FAP in the absence of substrates leads to irreversible inactivation.[12]

Enzyme-membrane reactors have received extensive attention in the field of photobiological culture.[13] Due to their large specific surface area, the membrane carriers exhibit a favourable propensity for light capture.[14] Additionally, the flow regime generates turbulence on the membrane surface and facilitates mass transfer.[15,16] Flow-chemistry applications on FAPs are scarce and limited to soluble enzymes.[12,17] Furthermore, FAP studies so far have almost exclusively on the prototypal FAP from *Chlorella variabilis* (*Cv*FAP). Due to its preference for long chain fatty acids, limiting its broad applicability for biomass-derived fatty acids.[18,19]
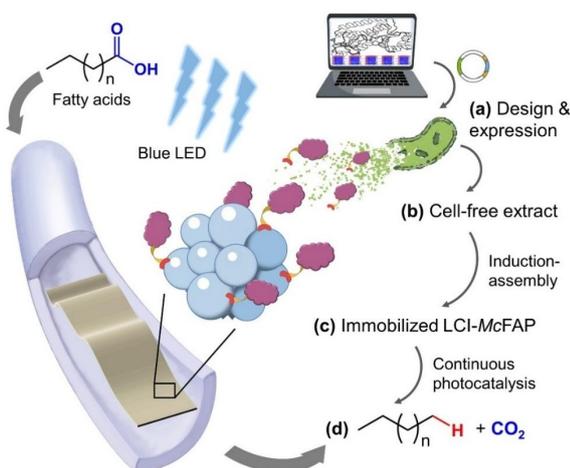
Interestingly, wild-type FAP contains an *N*-terminal transit peptide directing it to the chloroplast membrane.[20,21] In procaryotic expression systems such as *Escherichia coli* (*E. coli*) this transit peptide impairs heterologous expression and therefore is generally removed.[22] This natural self-assembly tendency of FAP inspired us to evaluate FAP-immobilization on synthetic membranes. As these membranes are generally chemically inert, they also lack suitable anchoring sites for e.g. covalent enzyme immobilization.[23,24] We therefore decided to evaluate polymer-binding peptides (PBPs), also known as material-binding peptides, for the directional immobilization of FAP to a modified membrane surface.[25] By genetically combining FAP to PBPs, a self-immobilizing fusion protein for application in flow was envisioned (Scheme 1).

[a] J. Zhou, Q. He, Prof. W. Chen, Dr. Y. Ma, Prof. Y. Wang
School of Food Science and Engineering
South China University of Technology
Guangzhou 510640 (China)
E-mail: myj605740779@scut.edu.cn
        yonghw@scut.edu.cn

[b] Prof. F. Hollmann
Department of Biotechnology
Delft University of Technology
van der Maasweg 9, 2629HZ, Delft (The Netherlands)

[c] Prof. Y. Wang
Guangdong Youmei Institute of Intelligent Bio-manufacturing Co. Ltd
Foshan, Guangdong 528200 (China)

ChemSusChem

Research Article
doi.org/10.1002/cssc.202301326

**Chemistry
Europe**
European Chemical
Societies Publishing

Scheme 1. Design of LCI–*Mc*FAP fusion protein, its immobilization on modified membranes and application in flow reactors.

As FAP, we chose for the FAP from *Micractinium conductrix* (*Mc*FAP) mainly for its broad fatty acid substrate spectrum.[26] As fusion PBP we chose for the LCI (liquid chromatography peak I) peptide from *Bacillus subtilis*.[27,28] LCI is a highly cationic peptide,[29] which should ensure a high affinity of the resulting fusion protein to negatively charged surfaces. To obtain such a surface, we chose a polyvinylidene fluoride (PVDF) membrane to be surface-modified by a layer-by-layer assembly process.

Results and Discussion

Design and synthesis of functionalized membranes

To enable the binding of the enzyme through electrostatic interaction, we performed a surface modification of PVDF membranes (Scheme 2). Our strategy aimed enabling binding of LCI–*Mc*FAP to PVDF, specifically by expanding the surface
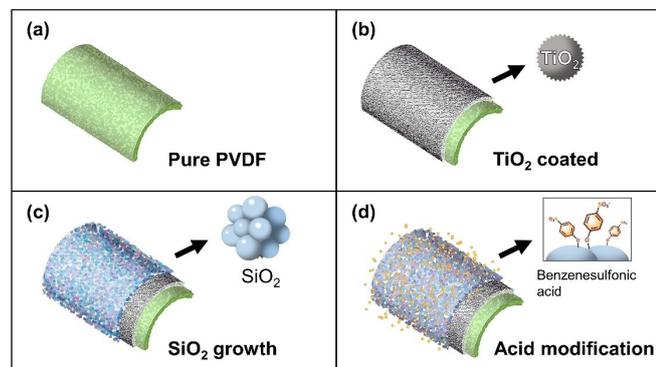
Scheme 2. Design of functionalized membranes. (a) **PVDF** membrane as support (pore size 0.45 µm); (b) TiO$_2$ coating provided active hydroxyl groups and nucleation sites, **PVDF-Ti**; (c) in situ growth of SiO$_2$ nanoscale particles to increase the effective surface area, **PVDF-Ti-Si**; (d) covalent coating with 4-chlorobenzene sulfonic acid to attain overall negatively charged surfaces, **PVDF-Ti-Si-SO$_3$H**.

area and adding additional negative charges. The sol-gel coated PVDF membrane was been demonstrated to stably bind nano-scale TiO$_2$ on its surface.[30] We optimized the protocol to reduce the number of coating cycles compared to the original process.[31] To further increase the surface area, we chose an *in situ* SiO$_2$ growth method. The TiO$_2$ coated membrane was more conducive to the adhesion and growth of SiO$_2$, shortening the tetraethyl orthosilicate (TEOS) solution's turbidity transition time to about 2 h (compared to 8 h for untreated PVDF membrane, see Figure S1). To attain the desired negatively charged surface, the final step involved partially modifying the silicone hydroxyl groups with 4-chlorobenzene sulfonic acid (as indicated by elemental distribution in Figure 1e). The coated surface was densely packed with nanosized silica, including capillary action and displaying superhydrophilicity (as shown in the water contact angle test in Figure 1f–i).

Design and expression of modified McFAP

Short-length *Mc*FAP (amino acid residues 551–1146) was first designed to achieve heterologous expression for subsequent experiments. Then, we utilized the cationic antimicrobial peptide derived from *Bacillus subtilis* to replace the *N*-terminal transit peptide of *Mc*FAP, creating LCI–*Mc*FAP. To ensure that
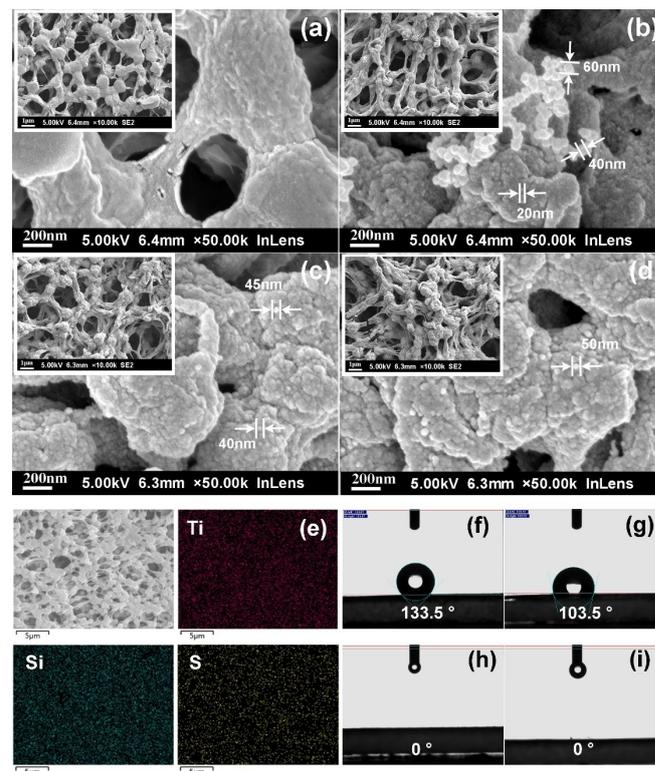
Figure 1. Characterization of functionalized membranes. (a-d) SEM image of the membranes, (a) **PVDF**, (b) **PVDF-Ti**, (c) **PVDF-Ti-Si**, (d) **PVDF-Ti-Si-SO$_3$H**; (e) Energy Dispersive Spectroscopy (EDS) analysis of **PVDF-Ti-Si-SO$_3$H** membrane surface: distribution of Ti, Si and S on the membrane surface; (f-i) Water contact angles for the different materials: (f) **PVDF**; (g) **PVDF-Ti**; (h) **PVDF-Ti-Si**; (i) **PVDF-Ti-Si-SO$_3$H**. Droplets were absorbed instantaneously in case of **PVDF-Ti-Si**; (i) **PVDF-Ti-Si-SO$_3$H**.

substrate access to the enzyme's active site remains unaffected, LCI was separated from *Mc*FAP by a rigid, α-helix-forming linker (EAAAK)₃. We also designed a fusion protein, *Mc*FAP-LCI, by combining the truncated *Mc*FAP *C*-terminally with LCI. Alpha-Fold2 was used to model the three-dimensional structures of all modified proteins (Figure 2). We conducted a local structural comparison (Figure 2a(i)), confirming that the substrate channel of LCI–*Mc*FAP remained unblocked. Moreover, the *N*-terminus of *Mc*FAP contained multiple groups of α-helix and β-sheet, potentially contributing to the conformational stability of the fusion protein (Figure 2a(ii)). Based on the protein folding confidence score, LCI–*Mc*FAP demonstrated a higher overall score compared to *Mc*FAP-LCI, suggesting that the former folding was more reasonable and had a more stable configuration (Figure 2a(iii) and Figure 2b(iii), respectively). The theoretical isoelectric point of *Mc*FAP was 8.6, whereas that of LCI was 10.3. LCI presents alkaline lysine and arginine residues at its subunit surface (Figure 2c(i–iii)), leading to the hypothesis that the fusion proteins will preferentially bind to polar surfaces via interaction with the newly introduced LCI subunit.

Both fusion proteins were successfully expressed in *E. coli* (Figure S2a–b). The fusion proteins exhibited a molecular weight around 72 kDa, consistent with the calculated molecular weight. Next, the enzyme activities of the purified proteins were determined. Compared to the parent enzyme, LCI–*Mc*FAP showed no significant difference in caprylic acid decarboxylation activity (Figure S2c). However, in the case of *Mc*FAP fused with LCI at the *C*-terminus (*Mc*FAP-LCI), the specific enzyme activity of the fusion protein decreased, and the yield dropped to only 2.4%. These experimental results aligned with the theoretical protein model, leading us to select LCI–*Mc*FAP for further study.

Induction-assembly between membranes and enzyme

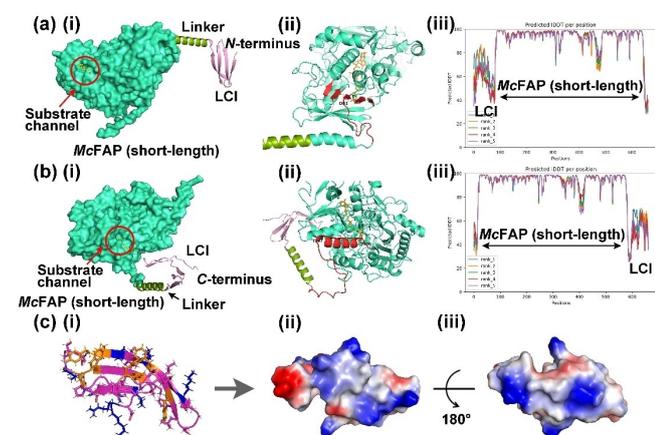To determine the optimal immobilization time, the adsorption characteristics of four types of membranes on proteins were investigated (see Figure S4 for the immobilization process). Initially, crude enzyme extracts of *Mc*FAP or LCI–*Mc*FAP were used to monitor the total protein concentration. The hydrophobic PVDF membrane exhibited minimal protein adsorption. In contrast, the functionalized membranes showed enhanced adsorption of proteins (Figure 3). Particularly, the membrane functionalized with benzenesulfonic acid (**PVDF-Ti-Si-SO₃H**) demonstrated a significantly shortened immobilization time (about 8 h), attributed to the attractive interaction of the target protein and the membrane. SDS-PAGE analysis revealed that the **PVDF-Ti-Si-SO₃H** membrane group had the most substantial reduction in free enzyme content (relative gray calculation content decreased by 10%, see Figure S3), followed by the **PVDF-Ti-Si** membrane.

Fluorescence assays were employed to demonstrate the immobilization of the target protein on the membrane, followed by testing the loading capacity of proteins on the membrane. Initially, a spectral scan was performed to determine the specific emission spectrum of the purified target protein, eliminating any background interference. The emission wavelengths of the target proteins were determined around 520–570 nm, exhibiting green fluorescence with no significant difference between LCI–*Mc*FAP and *Mc*FAP. On the other hand, the *E. coli* extract without target proteins did not exhibit any fluorescence (see Figure S4b–d). The immobilization of LCI–*Mc*FAP on the **PVDF-Ti-Si-SO₃H** membrane was observed over time using laser confocal microscopy. The fluorescence intensity reached a maximum between 8–12 h (see Figure S4e), which was consistent with the trend of protein concentration observed in Figure 3d. Therefore, we concluded that the immobilization time should be set at 12 h. Based on the comparison of fluorescence intensity across different samples, we identified **PVDF-Ti-Si-SO₃H** as the best membrane for enzyme immobilization (Figure 4e, there were 5 mg of protein attached to each square centimeter). The membranes coated

Figure 2. Modelled protein structures. (**a**) overall structure of LCI–*Mc*FAP, (**b**) overall structure of *Mc*FAP-LCI, (**c**) LCI composition: (i) lysine and arginine residues, (ii) charge distribution within LCI: positive: blue, negative: red, neutral: grey.[29]
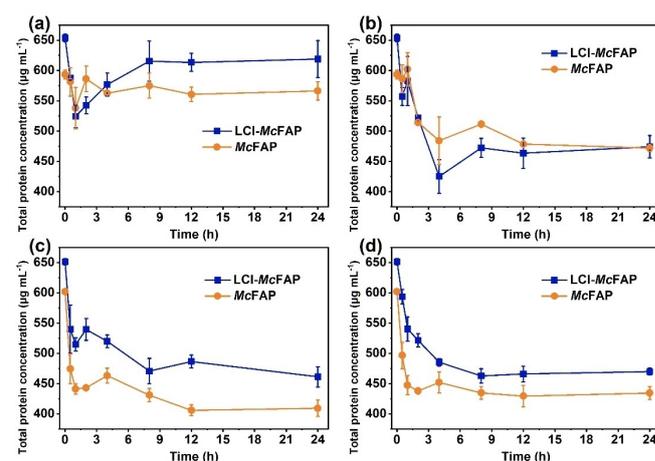
Figure 3. Time courses of protein adsorption (based on the determination of the soluble protein content). LCI–*Mc*FAP (yellow) and *Mc*FAP (blue). (a) **PVDF**; (b) **PVDF-Ti**; (c) **PVDF-Ti-Si**; (d) **PVDF-Ti-Si-SO₃H**. Per 1 cm² membrane 1.5 mL of crude extract solution was added and incubated by rotating incubator (20 r min⁻¹), 4 °C. Soluble protein concentrations were using the Bradford scheme (Coomassie brilliant blue staining).
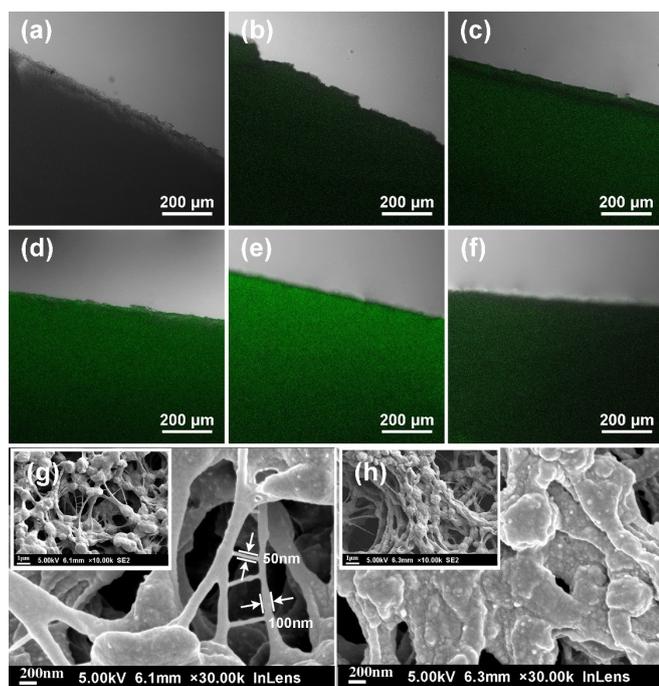
ChemSusChem

Research Article
doi.org/10.1002/cssc.202301326

Chemistry
Europe
European Chemical
Societies Publishing

Figure 4. Laser confocal microscope images of protein-coated membranes (a-f) and surface morphology (g,h) of **PVDF-Ti-Si-SO₃H** membrane after immobilization. (a) the **PVDF-Ti-Si-SO₃H** coated with *E. coli* extract of cells not containing LCI–*Mc*FAP (negative control), LCI–*Mc*FAP from *E. coli* crude extracts (total protein 4.1 mg mL^{-1}) on (b) **PVDF**, (c) **PVDF-Ti**, (d) **PVDF-Ti-Si** and (e) **PVDF-Ti-Si-SO₃H**. (f) *Mc*FAP (devoid of LCI) on **PVDF-Ti-Si-SO₃H** membrane. (g, h) Surface morphology of samples (e) and (f) using SEM, respectively.

with LCI–*Mc*FAP crude enzyme extract exhibited a large number of filamentous protein substances with a diameter of 50–100 nm, as observed in SEM images, and SiO₂ particles were covered entirely by protein filaments (Figure 4g). In contrast, a significant quantity of SiO₂ particles was found on the membrane covered by *Mc*FAP crude enzyme extract while no apparent *Mc*FAP filaments were present (Figure 4h), indicating that *Mc*FAP was less capable of adhering.

Photocatalytic experiments using the photoenzyme-membranes

Optimization of the immobilization conditions

We compared the catalytic activity of four types of membranes using caprylic acid as a substrate (Figure 5). **PVDF-Ti-Si-SO₃H** exhibited the highest performance in both *Mc*FAP and LCI–*Mc*FAP extracts (Figure 5a). This could be related to the membrane surface's electronegativity and hydrophilicity, which increased the quantity of enzyme attachment and mass exchange. In the next step, we varied the protein concentration of the crude enzyme extract for immobilization. Figure 5b shows that when the total protein concentration reached or exceeded 3 mg mL^{-1}, the conversion capacity did not increase further. To summarize the aforementioned findings, we chose
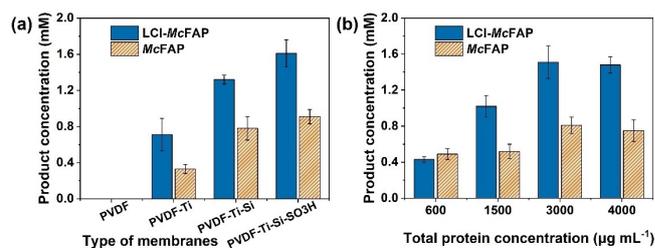

Figure 5. Decarboxylation of caprylic acid by functionalized membranes treated with crude enzyme extracts. 1 cm² of the modified membrane was added to each vial containing 10 mM caprylic acid. Total volume 1 mL, 15 % v/v DMSO, 25 °C, 400 rpm, 6 h, blue LED (photosynthetic photon flux density, PPFD = 791.2 μmol s^{-1} m^{-2}). (a) different membranes coated with proteins (total protein concentration 4.4 mg mL^{-1}, 0.39 U mL^{-1} for LCI–*Mc*FAP extracts; 4.2 mg mL^{-1}, 0.50 U mL^{-1} for *Mc*FAP extracts), (b) catalytic effects of **PVDF-Ti-Si-SO₃H** membrane treated with different protein concentrations of extracts.

LCI–*Mc*FAP with the stronger adhesion and hydrophilic **PVDF-Ti-Si-SO₃H** membrane with a negative charge surface as the carrier for subsequent studies.

Comparison of the catalytic activity and substrate scope of free and immobilized LCI–*Mc*FAP

According to the biotransformation results of free enzyme LCI–*Mc*FAP on fatty acids with different carbon numbers (Figure 6a), the fusion protein exhibited affinity for both medium and long chain fatty acids. However, it notably favored palmitic acid, which differed from the previous report on *Mc*FAP.[26] Remarkably, a mere 200 μL extract (total protein concentration
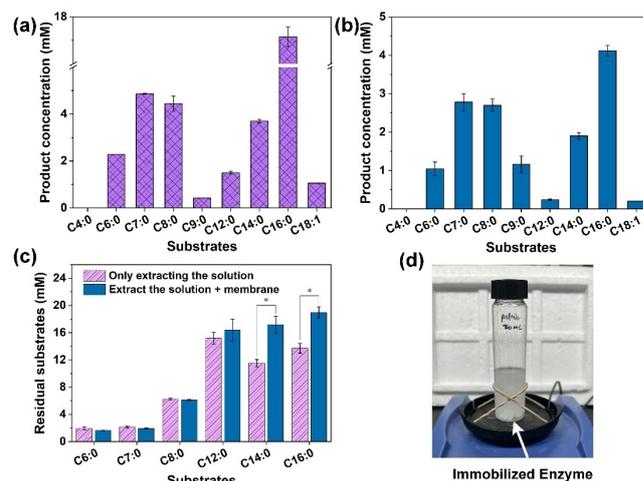

Figure 6. Activity of LCI–*Mc*FAP for different fatty acids in the free or immobilized enzyme (in batch). (a) free LCI–*Mc*FAP (200 μL) was added to the vial. (b) immobilized LCI–*Mc*FAP on **PVDF-Ti-Si-SO₃H** membrane (1 cm² of modified membrane) was added to the vial. (c) estimation of the amount of fatty acids absorbed on the membrane, (d) palmitic acid precipitation in reaction (immobilized enzyme as catalyst). Reaction conditions: medium chain fatty acids (C4:0–C9:0) = 20 mM and contained 15 % (v/v) DMSO; long chain fatty acids (C12:0–C18:1) = 20 mM and contained 30 % (v/v) DMSO, Tris-HCl buffer (100 mM, pH 8.5), total volume = 1 mL, 25 °C, 400 rpm, 6 h.

ChemSusChem

Research Article
doi.org/10.1002/cssc.202301326

**Chemistry
Europe**
European Chemical
Societies Publishing

4.0 mg mL^{-1}, 0.32 U for caprylic acid) converted 85.8% of palmitic acid (20 mM) into *n*-pentadecane.

We selected LCl–*Mc*FAP-**PVDF-Ti-Si-SO₃H** to explore the substrate scope of the immobilized enzyme. Similar to the free enzyme, LCl–*Mc*FAP-**PVDF-Ti-Si-SO₃H** demonstrated an affinity for both medium and long chain fatty acids, but the conversion of long chain fatty acids (especially to palmitic acid) was weaker (Figure 6b). To explain this result, we evaluated the residual amounts of substrates at the end of the reaction and discovered that long chain fatty acids tended to be absorbed by the membrane, whereas medium chain fatty acids were evenly distributed throughout the system (Figure 6c). Following that, palmitic acid was used as a substrate for further testing. It was apparent that as the reaction progressed, palmitic acid precipitation caused the fluid to change from clear to milky white (Figure 6d). On the contrary, no precipitation occurred with medium chain fatty acids.

It can be inferred that long chain fatty acids were more likely to be absorbed by the photoenzyme-membranes, leading to local concentrations surpassing the solubility limit, which may be related to the typically low critical micelle concentration of long chain fatty acids.[32] Consequently, long chain fatty acids precipitation occurred and hindered the reaction. On the other hand, the medium chain fatty acids, being more ionized in the alkaline buffer, experienced electrostatic repulsion from the **PVDF-Ti-Si-SO₃H** membrane, preventing their accumulation and enabling the reaction to proceed without precipitation.

Figure 7. Time courses and recycling experiments (in batch) of LCl–*Mc*FAP-**PVDF-Ti-Si-SO₃H** immobilized enzyme. (a) time course of catalytic reaction. (b) fluorescence attenuation of the photoenzyme-membrane surface during photocatalysis with continuous magnetic stirring (caprylic acid as substrate). (c) photoenzyme-membrane recycling experiment. Reaction conditions: 1 cm² of immobilized enzyme was added to the vial, caprylic acid = 10 mM (15% v/v DMSO) or palmitic acid = 10 mM (25% v/v DMSO), Tris-HCl buffer (100 mM, pH 8.5), total volume = 1 mL, 25 °C, 400 rpm.

Time course and recycling of LCl–*Mc*FAP photoenzyme-membrane

Next, we investigated the stability and recyclability of the LCl–*Mc*FAP photoenzyme-membrane. Caprylic acid and palmitic acid, representing medium and long chain fatty acids, respectively, were used in the subsequent experiments. As shown in Figure 7a, the decarboxylation rates of caprylic acid and palmitic acid decreased substantially after 1 h. To rule out the possibility that the decrease in the catalytic rate at this time was due to enzyme inactivation or leaching, we repeated the process and observed the changes in immobilized enzyme fluorescence at distinct reaction time points using confocal laser microscopy. Through continuous agitation in the vials, as shown in Figure 7b, the fluorescence on the photoenzyme-membrane surface did not decrease from the beginning of the reaction to 2 h, indicating that LCl–*Mc*FAP was steadfastly attached to the membrane without deactivation (deactivated FAP had no fluorescence). The fluorescence decreased only after 4 h. Therefore, the decreased catalytic rate at 1 h, is most likely due to the inhibition of product or precipitation of long chain fatty acids. As a result, we decided to terminate the reaction and extract the product after one hour.

Based on setting 1 h as a cycle, we attempted recycling the immobilized enzyme for consecutive cycles. As shown in Figure 7c, the enzyme could be reused at least 5 times, though its catalytic activity decreased with each recycle. It is worth
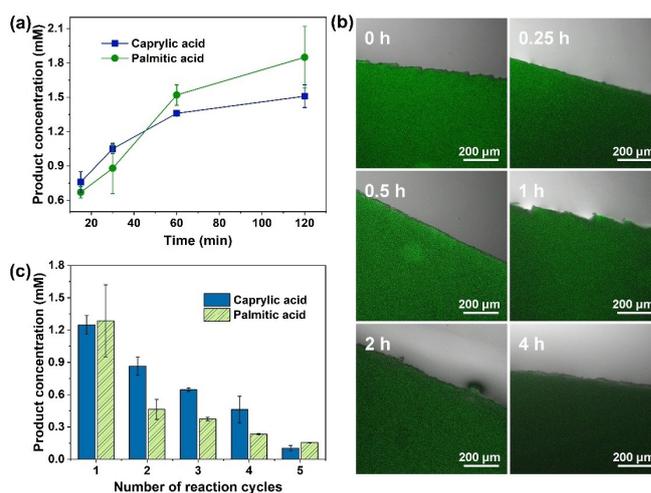
noting that caprylic acid also delayed enzyme inactivation, similar to the previously reported in free *Cv*FAP.[33]

Construction of a continuous photocatalytic flow reactor

To increase the surface-to-reaction ratio, we placed the LCl–*Mc*FAP-**PVDF-Ti-Si-SO₃H** photoenzyme-membrane inside a fluorinated ethylene propylene (FEP) tube (Figure 8a) to construct a mesoscale reactor. By doing this, the membrane appeared translucent in an environment containing DMSO, intending to eliminate poor enzyme illumination as an overall rate-limiting factor. Based on the results of batch testing, the catalytic rate decreased rapidly after 1 h of reaction. Therefore, the photocatalytic time in the continuous flow reactor was set to 1 h for each cycle while the photosynthetic photon flux density (PPFD) remained at 791.2 μmol s^{-1} m^{-2}. It is worth noting that with the increased liquid flow rate in the pipeline, the conversion of fatty acids also increased correspondingly (Figure 8c), which might be related to the acceleration of substance exchange and delayed hydrophobicity at the solid-liquid interface. Under continuous illumination conditions, the catalytic activity of the photoenzyme-membrane decreased steadily upon re-use. This decrease was more pronounced in case of palmitic acid as the starting material, possibly due to the poorer solubility of the reactants as discussed above. With caprylic acid as the substrate, the highest space time yield reached 1.2 mmol L^{-1} h^{-1} (*n*-heptane) (Figure 8d).

Changing the illumination strategy from continuous exposure to pulsed illumination (Figure 8e, blue LED operated in an alternating on/off program with a cycle of 1.0 s, i.e., reducing the overall light exposure of the enzyme by 50%) had a
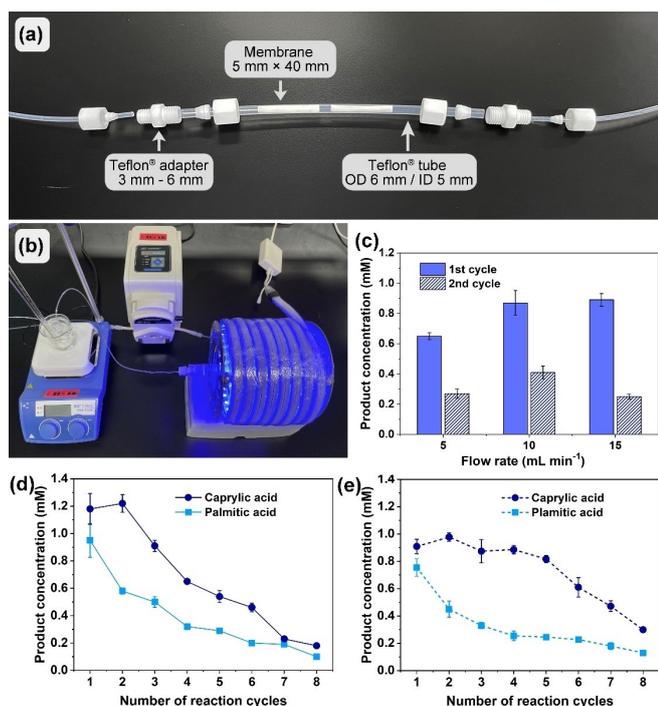
ChemSusChem

Research Article
doi.org/10.1002/cssc.202301326

**Chemistry
Europe**
European Chemical
Societies Publishing

Figure 8. Construction and application of photoenzyme-membrane flow catalytic equipment. (a) Components of parts exposed to blue light. (b) frontal view of the photocatalytic system, including a thermostatic magnetic stirrer (left), a peristaltic pump (centre, pump tube with PTFE lining), and an illuminated section (right). (c) correlation between flow rate and production concentration (10 mM palmitic acid as substrate, 1 h for each cycle). LCI–*Mc*FAP-**PVDF-Ti-Si-SO$_3$H** photoenzyme-membrane was placed in flow photocatalytic equipment (flow rate = 10 mL min^{-1}, 1 h for each cycle) for decarboxylating fatty acids under continuous illumination (d) and pulsed illumination (e), respectively.

somewhat stabilizing effect on the reactions converting caprylic acid. This illumination method enabled the photoenzyme-membrane to operate for at least eight cycles, possibly as a consequence of reduced light stress.[34] This stabilization effect suggested that the decrease in conversion was mainly due to light inactivation rather than enzyme leaching. In the case of palmitic acid, no stabilizing effect of pulsed illumination on the reaction was identified, possibly due to substrate precipitation and/or product (*n*-pentadecane) accumulation that has been mentioned, leading to inactivation of the enzyme. In addition, the light intensity in the continuous flow device needs to be further optimized, which is an important parameter for scalable preparation. The aforementioned experimental results are preferable to the previously reported immobilized continuous catalytic experiments (six effective cycles, accumulated running time of two hours[35]) pertaining to FAP and serve as a technical reference for the photobiocatalytic production of alkane biofuel or biochemicals.

Conclusions

A new approach was adopted to maximize light absorption capacity while concurrently preserving photoenzyme function-

ality, which was achieved by integrating the engineered assembled photoenzyme-membrane with a mesoscale illuminated flow device. Utilizing the inherent ability of FAP to be directed towards the biofilm through transit peptide in its natural state, the engineered *Mc*FAP variant can b e effectively attached to the artificial membrane surface stably, obviating the need for supplementary purification steps. The immobilized enzyme displayed remarkable adaptability across different fatty acids (C6–C18) in batch assessments, demonstrating robustness against mechanical and solvent-induced stresses. In subsequent endeavors involving continuous flow photocatalysis, the reactor system completed a total of eight effective cycles (the cumulative catalytic time was eight hours). This performance surpassed previously documented accomplishments of immobilized FAP. Furthermore, because there was no covalent bond between the matrical membrane (PVDF) and the modification component, recycling of the material was an option. The assembled photoenzyme-membrane catalytic configuration optimized the sustained usability of the photoenzyme and streamlined the photocatalytic synthesis of alkane biofuels.

Materials and methods

Materials: Hydrophobic polyvinylidene fluoride (PVDF) membrane with a pore size of 0.45 μm was purchased from Millipore (Shanghai) Ltd. Titanium isopropoxide (TTIP) (97%), tetraethyl orthosilicate (TEOS) (98%) and 4-chlorobenzenesulfonic acid hydrate (98%) were purchased from Aladdin Ltd., Shanghai, China. Ethyl acetate and other solvents were purchased from Macklin Ltd, Shanghai, China. *E. coli* TOP10 was used for constructing plasmids, *E. coli* BL21 (DE3) was used to heterologously express enzymes. Water was purified with a Millipore (Bedford, MA) Milli-Q water system.

Synthesis of functionalized membranes

PVDF-Ti membrane: The PVDF membrane was pre-soaked in deionized water and ethanol for 24 h, respectively, to remove preservatives. The titanate sol-gel solution was prepared following reported methods.[31] The pre-treated PVDF membrane was then immersed in the sol solution for 10 s, and the membrane was uniformly withdrawn at 0.9 mm s^{-1}. The coating film was dried at 90 °C for 1 h and then transferred to an 80 °C water bath for 12 h to complete the hydrolysis. Finally, the membrane was washed with deionized water and dried at room temperature. This procedure was repeated once.

PVDF-Ti-Si membrane: 20 cm^2 of the **PVDF-Ti** membrane were immersed and stirred for 2 h at 25 °C, 500 rpm in a 40 mL of solution of ethanol: H$_2$O: ammonia: TEOS of 8.4:1.0:0.1:0.5 (volume ratio). The sample was washed with ethanol and deionized water, dried at 60 °C. The amount of SiO$_2$ precipitated was estimated gravimetrically.

PVDF-Ti-Si-SO$_3$H membrane: Depending on the amount of SiO$_2$ grown in the previous step, 4-benzenesulfonic acid (3 g g^{-1}

ChemSusChem

Research Article
doi.org/10.1002/cssc.202301326

Chemistry
Europe
European Chemical
Societies Publishing

(SiO$_2$)) was added for further modification following a previously reported procedure.[36]

Construction, expression and purification of *Mc*FAP or fusion proteins: Genes (see SI for sequences) were synthesized by Sangon Biotech (Shanghai) Co., Ltd. For *Mc*FAP a truncated variant (Δ1–550) was used. Between the *N*- or *C*-terminus of *Mc*FAP and LCI a (EAAAK)$_3$ repetitive sequence linker was placed, resulting in LCI–*Mc*FAP or *Mc*FAP-LCI respectively (Table S1), which were subsequently cloned into the vector pET28a. The plasmid vectors were transformed into *E. coli* BL21 (DE3) to produce the designed proteins. The enzyme was expressed and purified according to the reported procedure.[26,28]

Analysis of the protein concentration, enzyme activity, gas chromatography and protein structure simulation: Protein concentration: Coomassie brilliant blue staining (Bradford scheme), the absorption wavelength was 595 nm (bovine serum protein as standard) and was detected by 96-well plate with Cytation™ 5 Cell Imaging Multi-Mode Reader (Bio Tek Ltd. USA), calculated through Equation (1).

$$y = 0.0018x + 0.1179 \quad R^2 = 0.9903 \tag{1}$$

y: absorbance (a.u.), *x*: protein concentration (50~300 μg mL^{-1}).

Enzyme activity assay: 20 mM caprylic acid and 12 μM purified enzyme were dissolved in 100 mM Tris-HCl buffer (pH 8.5) containing 15% (v/v) DMSO to a total volume 1 mL. Assay reactions were performed at 25 °C, 500 rpm for 30 min, (PPFD = 791.2 μmol s^{-1} m^{-2}). For enzyme activity calculations Equation (2) was used.

$$X = \frac{n}{c \cdot V \cdot t} \tag{2}$$

X: enzyme activity (U mg^{-1}), *n*: amount of *n*-heptane (μmol), *c*: concentration of *Mc*FAP or fusion protein (mg mL^{-1}), *V*: volume of *Mc*FAP or fusion protein solution being added (mL), *t*: reaction time (min).

Gas chromatographic quantification: for a full description, please see Table S2.

Isoelectric points and molecular weights of the proteins were supported by the SIB Bioinformatics Resource Portal, ExPASy. (http://www.expasy.org/). The 3D structures of proteins were based on the AlphaFold2 operation.

General Procedure for the enzyme immobilization and fluorescence analysis: The cells were suspended in Tris-HCl 50 mM, pH 7.5, 100 mM NaCl and 5% w/v glycerol (buffer C) and disrupted by ultrasonic equipment (Xinzhi Biotechnology Co., Ltd., Ningbo. 60% power, 10 min of operation). The supernatant was collected by centrifugation (11000 g, 30 min). Total protein concentration was 4.4 mg mL^{-1}, 0.39 U mL^{-1} for LCI–*Mc*FAP extracts, and 4.2 mg mL^{-1}, 0.50 U mL^{-1} for *Mc*FAP extracts unless otherwise stated. Each functionalized membrane (1 cm^2) was immersed into a test tube containing crude enzyme extract (1.5 mL) and rotated in a refrigerator protected from light at a rotating incubator (20 rpm, 12 h at 4 °C). The membrane was then removed and washed with buffer C

(10 mL), stored at 4 °C. The coated membrane sample was placed on a slide and observed by a laser confocal microscope (Zeiss LSM710, Germany). The FAP on the membrane surface can be excited by 488 nm laser with an emission wavelength range of 520–570 nm; the gain of the signal was 400.

General Procedure for the biotransformation using free or immobilized enzyme

Batch experiments: Every photoenzyme-membrane (1 cm^2) was divided into small pieces and transferred to a buffer solution (100 mM Tris-HCl, pH 8.5) containing 10 mM fatty acid substrate and 15% (v/v) DMSO for a total volume of 1 mL in 4 mL transparent vial, unless stated otherwise. The vials were placed in a photocatalytic device and exposed to blue LED (photosynthetic photon flux density, PPFD = 791.2 μmol s^{-1} m^{-2}) for a pre-set time at 400 rpm, 25 °C. To extract also reactants absorbed on the membrane (Figure S5), the entire reaction including membranes was extracted with ethyl acetate (1 mL, containing 5 mM *n*-octanol as the internal standard). For reusability analysis, when all the solution was removed, a new reaction solution was added to the vial and started the next cycle. After centrifugation (12000 g, 3 min), organic phases were collected for gas chromatography analysis.

Continuous flow reaction system: The tube (internal diameter 5 mm, external diameter 6 mm, length 200 mm) was washed with buffer (100 mM Tris-HCl, pH 8.5) in advance, then filled with the photoenzyme-membrane (total 8 cm^2). Next, reaction solution (8 mL) containing 10 mM fatty acids and DMSO (15% v/v for caprylic acid or 25% v/v for palmitic acid) was perfused through peristaltic pump and kept circulating for 1 h at a specific flow rate (PPFD = 791.2 μmol s^{-1} m^{-2}, continuous or pulsed illumination). At the end of the reaction, ethyl acetate (8 mL, containing 5 mM *n*-octanol) was injected into the tube and all the liquid was recovered. After all the liquid had been drained, a new reaction solution (8 mL) was perfused and started the next cycle.

Supporting Information

Supporting information is available for this article including membrane modification process, sequence information, enzyme purification (activity testing), immobilization process.

Author Contributions

J. Zhou, Q. He and Y. Ma conceived, designed the study, and performed the experiments, J. Zhou, Y. Ma and Y. Wang analyzed the experimental data. F. Hollmann and W. Chen assisted in data interpretation and manuscript formulation. All the authors contributed to scientific discussion. The article was written based on contributions from all authors.

Conflict of Interests

The authors declare no conflict of interest. Guangdong Youmei Institute of Intelligent Bio-manufacturing Co., Ltd provides some experimental instruments for testing during the whole experiment process. The company will not have any conflicts of interest.

Data Availability Statement

The data that support the findings of this study are available from the corresponding author upon reasonable request.
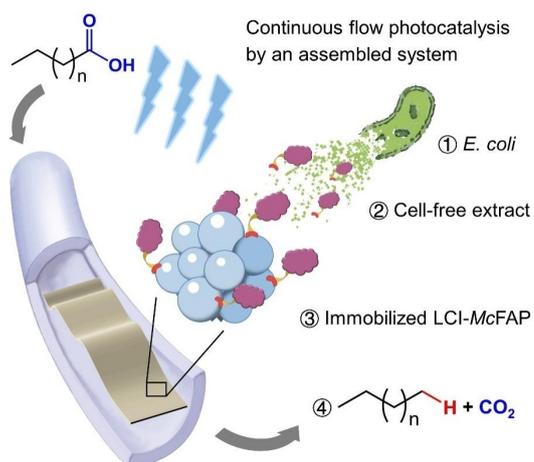
[1] M. V. Rodionova, R. S. Poudyal, I. Tiwari, R. A. Voloshin, S. K. Zharmukha-medov, H. G. Nam, B. K. Zayadan, B. D. Bruce, H. J. M. Hou, S. I. Allakhverdiev, *Int. J. Hydrogen Energy* **2017**, *42*, 8450–8461.

[2] M. Hasan, M. Z. Abedin, M. B. Amin, Md. Nekmahmud, J. Oláh, *J. Environ. Manage.* **2023**, *336*, 117644.

[3] A. Sarwer, M. Hussain, A. H. Al-Muhtaseb, A. Inayat, S. Rafiq, M. S. Khurram, N. Ul-Haq, N. S. Shah, A. Alaud Din, I. Ahmad, F. Jamil, *ChemBioEng Rev.* **2022**, *9*, 423-441.

[4] X. Guo, A. Xia, W. Zhang, Y. Huang, X. Zhu, X. Zhu, Q. Liao, *Bioresour. Technol.* **2023**, *367*, 128232.

[5] M. J. Barbosa, M. Janssen, C. Südfeld, S. D'Adamo, R. H. Wijffels, *Trends Biotechnol.* **2023**, *41*, 452–471.

[6] M. Abdul Hakim Shaah, Md. S. Hossain, F. A. Salem Allafi, A. Alsaedi, N. Ismail, M. O. Ab Kadir, M. I. Ahmad, *RSC Adv.* **2021**, *11*, 25018.

[7] D. Sorigué, K. Hadjidemetriou, S. Blangy, G. Gotthard, A. Bonvalet, N. Coquelle, P. Samire, A. Aleksandrov, L. Antonucci, A. Benachir, S. Boutet, M. Byrdin, M. Cammarata, S. Carbajo, S. Cuiné, R. B. Doak, L. Foucar, A. Gorel, M. Grünbein, E. Hartmann, R. Hienerwadel, M. Hilpert, M. Kloos, T. J. Lane, B. Légeret, P. Legrand, Y. Li-Beisson, S. L. Y. Moulin, D. Nurizzo, G. Peltier, G. Schirò, R. L. Shoeman, M. Sliwa, X. Solinas, B. Zhuang, T. R. M. Barends, J.-P. Colletier, M. Joffre, A. Royant, C. Berthomieu, M. Weik, T. Domratcheva, K. Brettel, M. H. Vos, I. Schlichting, P. Arnoux, P. Müller, F. Beisson, *Science* **2021**, *372*, eabd5687.

[8] D. Sorigué, B. Légeret, S. Cuiné, P. Morales, B. Mirabella, G. Guédeney, Y. Li-Beisson, R. Jetter, G. Peltier, F. Beisson, *Plant Physiol.* **2016**, *171*, 2393–2405.

[9] M. M. E. Huijbers, W. Zhang, F. Tonin, F. Hollmann, *Angew. Chem. Int. Ed.* **2018**, *130*, 13836–13839.

[10] B. O. Burek, A. Sutor, D. W. Bahnemann, J. Z. Bloh, *Catal. Sci. Technol.* **2017**, *7*, 4977–4983.

[11] S. N. Chanquia, F. Vig Benfeldt, N. Petrovai, P. Santner, F. Hollmann, B. E. Eser, S. Kara, *ChemBioChem* **2022**, *23*, e202200482.

[12] W. Z. Ng, E.-S. Chan, W. Gourich, C. W. Ooi, B. T. Tey, C. P. Song, *Renewable Sustainable Energy Rev.* **2023**, *184*, 113548.

[13] J. Li, R. Ou, H. Liao, J. Ma, L. Sun, Q. Jin, D. He, Q. Wang, *Sci. Total Environ.* **2022**, *851*, 158063.

[14] S. S. Rosli, W. N. Amalina Kadir, C. Y. Wong, F. Y. Han, J. W. Lim, M. K. Lam, S. Yusup, W. Kiatkittipong, K. Kiatkittipong, A. Usman, *Renewable Sustainable Energy Rev.* **2020**, *134*, 110306.

[15] Y. Luan, Y. Xu, Z. Guo, Y. Yin, Q. Wang, F. Zhang, Y. Xiao, C. Liu, S. Jiang, *Bioresour. Technol.* **2023**, *385*, 129426.

[16] C. Sambiagio, T. Noël, *Trends Chem.* **2020**, *2*, 92–106.

[17] F. Li, A. Xia, X. Guo, W. Zhang, Y. Huang, X. Zhu, X. Zhu, Q. Liao, *J. Environ. Chem. Eng.* **2023**, *11*, 110748.

[18] P. P. Samire, B. Zhuang, B. Légeret, Á. Baca-Porcel, G. Peltier, D. Sorigué, A. Aleksandrov, F. Beisson, P. Müller, *Sci. Adv.* **2023**, *9*, eadg3881.

[19] W. Zhang, M. Ma, M. M. E. Huijbers, G. A. Filonenko, E. A. Pidko, M. Van Schie, S. De Boer, B. O. Burek, J. Z. Bloh, W. J. H. Van Berkel, W. A. Smith, F. Hollmann, *J. Am. Chem. Soc.* **2019**, *141*, 3116–3120.

[20] C. Aselmeyer, B. Légeret, A. Bénarouche, D. Sorigué, G. Parsiegla, F. Beisson, F. Carrière, *Biochemistry* **2021**, *60*, 3200–3212.

[21] S. L. Y. Moulin, A. Beyly-Adriano, S. Cuiné, S. Blangy, B. Légeret, M. Floriani, A. Burlacot, D. Sorigué, P.-P. Samire, Y. Li-Beisson, G. Peltier, F. Beisson, *Plant Physiol.* **2021**, *186*, 1455–1472.

[22] Y. Zeng, X. Yin, L. Liu, W. Zhang, B. Chen, *Molecular Catalysis* **2022**, *532*, 112717.

[23] Y. Cen, Y. Liu, Y. Xue, Y. Zheng, *Adv. Synth. Catal.* **2019**, *361*, 5500–5515.

[24] F. Asaduzzaman, S. Salmon, *Mol. Syst. Des. Eng.* **2022**, *7*, 1385–1414.

[25] Y. Ruan, Y. Sohail, J. Zhao, F. Hu, Y. Li, P. Wang, L. Zhang, *ACS Biomater. Sci. Eng.* **2022**, *8*, 4738–4750.

[26] Y. Ma, X. Zhong, B. Wu, D. Lan, H. Zhang, F. Hollmann, Y. Wang, *Chin. J. Catal.* **2023**, *44*, 160–170.

[27] K. Rübsam, M. Davari, F. Jakob, U. Schwaneberg, *Polymer* **2018**, *10*, 423.

[28] K. Rübsam, B. Stomps, A. Böker, F. Jakob, U. Schwaneberg, *Polymer* **2017**, *116*, 124–132.

[29] W. Gong, J. Wang, Z. Chen, B. Xia, G. Lu, *Biochemistry* **2011**, *50*, 3621–3627.

[30] S. Meng, J. Mansouri, Y. Ye, V. Chen, *J. Membr. Sci.* **2014**, *450*, 48–59.

[31] J. Hou, G. Dong, Y. Ye, V. Chen, *J. Membr. Sci.* **2014**, *469*, 19–30.

[32] M. S. Akhter, *Colloids Surf. A* **1997**, *121*, 103–109.

[33] Y. Wu, C. E. Paul, F. Hollmann, *ChemBioChem* **2021**, *22*, 2420–2423.

[34] B. Lakavath, T. M. Hedison, D. J. Heyes, M. Shanmugam, M. Sakuma, R. Hoeven, V. Tilakaratna, N. S. Scrutton, *Anal. Biochem.* **2020**, *600*, 113749.

[35] S. Simić, M. Jakštaitė, W. T. S. Huck, C. K. Winkler, W. Kroutil, *ACS Catal.* **2022**, *12*, 14040–14049.

[36] H. Li, Q. Deng, H. Chen, X. Cao, J. Zheng, Y. Zhong, P. Zhang, J. Wang, Z. Zeng, S. Deng, *Appl. Catal. A* **2019**, *580*, 178–185.

RESEARCH ARTICLE

Continuous flow photocatalysis by an assembled system

① E. coli

② Cell-free extract

③ Immobilized LCI-McFAP

④ + CO_2

J. Zhou, Prof. F. Hollmann, Q. He, Prof. W. Chen, Dr. Y. Ma*, Prof. Y. Wang*

Continuous Fatty Acid Decarboxylation using an Immobilized Photodecarboxylase in a Membrane Reactor

This is an assembled photoenzyme-loaded membrane mesoscale reactor based on the behavior of biomolecules in nature, which produces different chain-length alkane biofuels in an unreported continuous manner.